ICES REPORT 89-08

June 1989

Hybrid-Trefftz Quadrilateral Elements for Thick Plate Analysis

by

J. Petrolito

The Institute for Computational Engineering and Sciences
The University of Texas at Austin
Austin, Texas 78712

Reference: J. Petrolito, "Hybrid-Trefftz Quadrilateral Elements for Thick Plate Analysis", ICES REPORT 89-08, The Institute for Computational Engineering and Sciences, The University of Texas at Austin, June 1989.

HYBRID-TREFFTZ QUADRILATERAL ELEMENTS FOR THICK PLATE ANALYSIS

*J. Petrolito**

Department of Civil Engineering
University College
Australian Defence Force Academy
Campbell, A.C.T. 2600, Australia

SUMMARY

A family of thick plate quadrilateral elements is derived based on the Hybrid-Trefftz formulation. Exact solutions of the governing equations are used inside the element together with independent displacements and rotations on the boundary of the element. The element stiffness equations are derived using a modified hybrid-stress variational principle which enables all element matrices to be calculated using only boundary integrals. The resulting elements enable the accurate analysis of both thick and thin plate to be performed.

1. INTRODUCTION

Current research into the development of efficient thick plate elements has mostly concentrated on the use of an underlying thick plate theory, usually Mindlin's first-order shear deformation theory [1]. The use of Mindlin's theory allows independent approximations for the transverse deflection and normal rotations. More importantly, only C_0 continuity is required for the shape functions, which can be easily achieved. In this way, the development of C_1 continuous shape functions, demanded by thin plate theory and difficult to achieve, is avoided. Moreover, the formulation is applicable to both thick and thin plates.

Despite the simplicity of the approach, several problems can arise with thick plate elements. First is the possibility of locking in the thin plate limit. This problem can be eliminated by using either reduced or selective integration techniques, details of which are given in e.g., [2,3]. However, reduced integration schemes may cause the

*Currently visiting the Texas Institute for Computational Mechanics, The University of Texas at Austin, Austin, Texas 78712, U.S.A.

element stiffness matrix to be rank deficient, giving rise to the generation of spurious mechanisms. Methods of controlling such problems are the subject of current research, and reviews of available techniques are given in [2-6]. A recent promising approach involves the use of discrete shear constraints, e.g., [7-10].

In the context of thin plate analysis, Jirousek and Leon [11] introduced a Hybrid-Trefftz procedure in which the internal element approximations satisfy the governing equations of the problem. Inter-element continuity is achieved as in the standard hybrid-stress method [12] by introducing independent boundary displacements which are common to adjacent elements. The approach results in elements of high accuracy, and the method has since been further refined and extended [13-15].

The aim of the present work is to extend the method to thick plate analysis. Solutions of Mindlin's equations have recently been used [16] to derive a modified version of the thin plate ACM element [2] that is suitable for thick plate analysis. While the element performs well and does not suffer from either locking problems or spurious mechanisms, it is restricted to a rectangular shape, as was the original ACM element. In this paper, the solutions used in [16] are extended to higher orders and combined with the Hybrid-Trefftz formulation to produce a family of quadrilateral thick plate elements.

2. GOVERNING EQUATIONS

The governing equations of Mindlin's theory are summarized below using the notation of Fig. 1. The deformation of the plate is described by the transverse displacement of the middle surface, w, and the rotations about the x and y axes, namely θ_y and θ_x.

The generalized strains in the plate are given by

$$\boldsymbol{\varepsilon}_b = \begin{bmatrix} \partial/\partial x & 0 \\ 0 & \partial/\partial y \\ \partial/\partial y & \partial/\partial x \end{bmatrix} \begin{Bmatrix} \theta_x \\ \theta_y \end{Bmatrix} = \boldsymbol{L}\boldsymbol{\theta} \tag{1.a}$$

$$\boldsymbol{\varepsilon}_s = \begin{Bmatrix} \partial/\partial x \\ \partial/\partial y \end{Bmatrix} w - \boldsymbol{\theta} = \boldsymbol{\nabla} w - \boldsymbol{\theta} \tag{1.b}$$

where $\boldsymbol{\varepsilon}_b$ is the bending strain vector and $\boldsymbol{\varepsilon}_s$ is the shear strain vector. In the thin plate limit, $\boldsymbol{\varepsilon}_s = \mathbf{0}$.

Assuming a homogeneous, isotropic material, the constitutive relationships are

$$\boldsymbol{M} = \left\{ \begin{array}{c} M_x \\ M_y \\ M_{xy} \end{array} \right\} = -\frac{Et^3}{(1-\nu^2)} \left[\begin{array}{ccc} 1 & \nu & 0 \\ \nu & 0 & 0 \\ 0 & 0 & (1-\nu)/2 \end{array} \right] \boldsymbol{L\theta} = -\boldsymbol{DL\theta} \qquad (2.a)$$

$$\boldsymbol{Q} = \left\{ \begin{array}{c} Q_x \\ Q_y \end{array} \right\} = kGt\,(\nabla w - \boldsymbol{\theta}) \qquad (2.b)$$

where E is Young's modulus, ν is Poisson's ratio, $G = E/2(1+\nu)$ is the shear modulus, t is the plate thickness and k is a correction factor to account for the non-uniform distribution of the shear stresses across the depth of the plate. Commonly used values of k are $5/6$ and $\pi^2/12$.

The static equilibrium equations for the plate are

$$\boldsymbol{Q} = \boldsymbol{L}^T \boldsymbol{M} \qquad (3.a)$$

$$\nabla^T \boldsymbol{Q} + p = 0 \qquad (3.b)$$

The displacement form of the governing equations is obtained by combining (1)-(3), giving

$$kGt\,(\nabla w - \boldsymbol{\theta}) + \boldsymbol{DL\theta} = \boldsymbol{0} \qquad (4.a)$$

$$-\nabla^T \boldsymbol{L}^T \boldsymbol{DL\theta} + p = 0 \qquad (4.b)$$

For the development of solutions of Mindlin's equations, it is convenient to express the governing equations in an uncoupled form for w and $\boldsymbol{\theta}$, namely [17]

$$\nabla^4 w = \frac{p}{D} - \frac{\nabla^2 p}{kGt} \qquad (5.a)$$

$$\left(\frac{t^2}{12k}\nabla^2 - 1\right)\left(\frac{\partial p}{\partial x} - D\nabla^4 \theta_x\right) = 0 \qquad (5.b)$$

$$\left(\frac{t^2}{12k}\nabla^2 - 1\right)\left(\frac{\partial p}{\partial y} - D\nabla^4 \theta_y\right) = 0 \qquad (5.c)$$

where $D = Et^3/12(1-\nu^2)$, ∇^2 is the Laplacian operator and $\nabla^4 = \nabla^2\nabla^2$ is the biharmonic operator. The main point to note from (5) is that in the case when $p = 0$, w is biharmonic as is the case in thin plate theory. This fact can be used to develop solutions of (4) for the case when $p = 0$ that are valid for any value of t.

3. SOLUTIONS OF MINDLIN'S EQUATIONS

3.1 Homogeneous Solutions

We first consider homogeneous solutions (i.e., with $p = 0$) of (4). Equation (5) shows that w is biharmonic in this case. To derive a solution of (4) which is valid for both thick and thin plates, we seek a solution of θ in the form

$$\theta_x = w_{,x} + Rf_1(x,y) \tag{6.a}$$

$$\theta_y = w_{,y} + Rf_2(x,y) \tag{6.b}$$

where $R = D/kGt$ is the ratio of the flexural rigidity to the shear rigidity. In the thin plate limit ($R = 0$), (6) correctly models the constraint $\boldsymbol{\theta} = \nabla w$. Thus, no locking will occur in the elements developed below.

To establish the unknown functions f_1 and f_2, (6) is substituted into (4) and the resulting differential equations are solved. This gives

$$f_1(x,y) = w_{,xxx} + w_{,xyy} \tag{7.a}$$

$$f_2(x,y) = w_{,yyy} + w_{,xxy} \tag{7.b}$$

Thus, with f_1 and f_2 given by (7), any biharmonic function for w together with rotations given by (6) is a solution of the homogenous form of (4).

Many biharmonic functions are known [18]. For finite element calculations, it is convenient to use polynomial functions. Jirousek and Guex [14] have suggested the following generating sequence:

$$w_{k+1} = r^2 \mathrm{Re}\ z^k \tag{8.a}$$

$$w_{k+2} = r^2 \mathrm{Im}\ z^k \tag{8.b}$$

$$w_{k+3} = \mathrm{Re}\ z^{k+2} \tag{8.c}$$

$$w_{k+4} = \mathrm{Im}\ z^{k+2} \tag{8.d}$$

for $k = 0, 1, 2 \ldots$, where $z = x + iy$, $r^2 = x^2 + y^2$ and Re and Im denote the real and imaginary parts of a complex number.

The following points should be noted when using (8) to generate biharmonic polynomials in conjunction with the element formulation given below; see also [14]:

(1) For $k = 0$, (8) only generates three solutions since (8.a) and (8.b) give the same polynomial, namely $x^2 + y^2$.

(2) Following from (1), geometrical invariance of the internal approximation is obtained by using an odd number of solutions.

(3) The generated solutions from (8) lead to non-zero stresses, i.e., the rigid body components $w = 1$, x and y are excluded. This is necessary to ensure that the element flexibility matrix derived below is non-singular.

(4) To ensure good numerical conditioning of the element flexibility matrix, the coordinates x and y should be scaled, e.g., by dividing by the square root of the element area.

Thus, the use of (8) together with (6) generates solutions of the homogeneous form of Mindlin's equations. It should be noted, however, that only a small number of the generated terms are used in the element formulation. No attempt is made to generate macro type elements [19] which would enable a single element, in the limit, to be used for the entire region. In this case the generated sequence is not suitable since it is not complete.

3.2 Particular Solutions

A number of particular solutions for Mindlin's plate theory may be found in standard texts, e.g. [17]. For a uniform load, p, the following solution is used in this work

$$w = \frac{(x^2 + y^2 - 16R)(x^2 + y^2)p}{64D} \tag{9.a}$$

$$\theta_x = \frac{x(x^2 + y^2)p}{16D} \tag{9.b}$$

$$\theta_y = \frac{y(x^2 + y^2)p}{16D} \tag{9.c}$$

To treat general loading distributions, the point load solution [17] may be used together with suitable integration to model the actual loading distribution. A solution to a bilinear loading distribution was derived in this way in [16].

4. ELEMENT FORMULATION

The elements developed here are based on independent assumptions for the internal displacements and boundary displacements. In principle, an arbitrary number of elements of polygonal shape and varying orders may be derived. The elements developed here are all quadrilaterals with boundary aproximations varying up to a cubic order.

The element formulation, which is common to all elements, is considered first. The formulation follows the standard hybrid-stress approach [12] with some modifications since displacement solutions, rather than stress solutions, are available inside the element [14].

The internal element approximation is taken as

$$\boldsymbol{u} = \boldsymbol{P}\boldsymbol{\beta} + \boldsymbol{u}_o = \boldsymbol{u}_\beta + \boldsymbol{u}_o \tag{10}$$

where $\boldsymbol{u} = \{w, \theta_x, \theta_y\}$ is a vector of element displacements, $\boldsymbol{P}$ contains M Trefftz solutions generated using (6) and (8), $\boldsymbol{\beta}$ is a vector of unknown parameters and $\boldsymbol{u}_o$ is a particular solution associated with the applied load on the element.

Using (1) and (2), the stresses inside the element can be obtained as

$$\boldsymbol{\sigma} = \boldsymbol{T}\boldsymbol{\beta} + \boldsymbol{\sigma}_o = \boldsymbol{\sigma}_\beta + \boldsymbol{\sigma}_o \tag{11}$$

where $\boldsymbol{\sigma} = \{\boldsymbol{M}, \boldsymbol{Q}\}$. Independent displacements, $\tilde{\boldsymbol{u}}$, are introduced on the boundary of the element as

$$\tilde{\boldsymbol{u}} = \boldsymbol{N}\boldsymbol{q} \tag{12}$$

where $\boldsymbol{q}$ is a vector of element degrees of freedom. The displacement vector $\tilde{\boldsymbol{u}}$ is common to adjacent elements with the shape functions $\boldsymbol{N}$ only being defined on the element boundary.

For the present problem, the hybrid-stress functional [12] is

$$\Pi_H = \frac{1}{2}\int_A \boldsymbol{\sigma}^T \boldsymbol{D}_1^{-1}\boldsymbol{\sigma} dA - \oint_S \tilde{\boldsymbol{u}}^T \boldsymbol{\sigma}_n dS + \int_{S_\sigma} \tilde{\boldsymbol{u}}^T \overline{\boldsymbol{\sigma}}_n dS \tag{13}$$

where

$$\boldsymbol{D}_1 = \begin{bmatrix} \boldsymbol{D} & \boldsymbol{0} \\ \boldsymbol{0} & kGt\boldsymbol{I} \end{bmatrix} \tag{14}$$

I is a 2 × 2 unit matrix, σ_n are the stress components at the boundary, $\overline{\sigma}_n$ are the specified stress components on part S_σ of the total element boundary, S, and A is the area of the element.

The area integral in (13) may be converted into a boundary integral as follows. Using (11), the area integral can be written as

$$\frac{1}{2}\int_A \sigma^T D_1^{-1}\sigma dA = \frac{1}{2}\int_A \sigma_\beta^T D_1^{-1}\sigma_\beta dA + \int_A \sigma_\beta^T D_1^{-1}\sigma_o dA + \frac{1}{2}\int_A \sigma_o^T D_1^{-1}\sigma_o dA \quad (15)$$

The last term in (15) is a constant since it only depends on the applied loading. From Clapyron's theorem, we have

$$\frac{1}{2}\int_A \sigma_\beta^T D_1^{-1}\sigma_\beta dA = \frac{1}{2}\oint_S u_\beta^T \sigma_{\beta n} dS \quad (16.a)$$

$$\int_A \sigma_\beta^T D_1^{-1}\sigma_o dA = \oint_S u_o^T \sigma_{\beta n} dS \quad (16.b)$$

Substituting (15) and (16) into (13) gives

$$\Pi_H = \frac{1}{2}\oint_S u_\beta^T \sigma_{\beta n} dS + \oint_S u_o^T \sigma_{\beta n} dS - \oint_S \tilde{u}^T \sigma_n dS + \int_{S_\sigma} \tilde{u}^T \overline{\sigma}_n dS + \text{constant} \quad (17)$$

Using the form of Π_H given by (17) enables the element equations to be derived using only boundary integrals. Thus, arbitrarily shaped polygonal elements may be derived in a straightforward manner if required.

Substituting (10), (11) and (12) into (17) and ignoring the constant gives

$$\Pi_H = \frac{1}{2}\beta^T H\beta + \beta^T H_o - \beta^T Gq + q^T R \quad (18)$$

where

$$H = \oint_S P^T T_n dS \quad (19.a)$$

$$H_o = \oint_S T_n^T u_o dS \quad (19.b)$$

$$G = \oint_S T_n^T N dS \quad (19.c)$$

$$R = \int_{S_\sigma} N^T \overline{\sigma}_n dS \quad (19.d)$$

T_n is a matrix containing the stress component functions on the boundary and H is the element flexibility matrix and is symmetric. Setting the first variation of Π_H with respect to β to zero gives

$$H\beta + H_o - Gq = 0 \tag{20}$$

Since the parameters β are local to each element, (20) can be solved to give

$$\beta = H^{-1}(Gq - H_o) \tag{21}$$

Substituting (21) into (18) and ignoring another constant gives

$$\Pi_H = -\frac{1}{2}q^T K q + q^T L \tag{22}$$

where the element stiffness matrix and load vector are given by

$$K = G^T H^{-1} G \tag{23.a}$$

$$L = R + G^T H^{-1} H_o \tag{23.b}$$

The element formulation is now in a standard stiffness form, and assembly and solution of the element equations follows the usual finite element procedure.

The global stiffness equations give directly the nodal displacements and rotations. The internal variables β can then be found from (21). This enables the element stresses to be calculated from (11). It should be noted that internal displacements found from (10) will be in error by a rigid body component, since this component was excluded from the approximation given in (10).

Several options are available to remedy this if internal displacements are required. First, it is possible to use shape functions defined over the element that are consistent with the boundary variation assumed for $\tilde{u}$. This is perhaps the most straightforward approach. Second [14], the internal displacement approximation can be augmented with the missing rigid body component and expressed as

$$\overline{u} = u + \begin{Bmatrix} c_1 + c_2 x + c_3 y \\ c_2 \\ c_3 \end{Bmatrix} \tag{24}$$

where c_1, c_2 and c_3 are unknown constants. These constants may be found by, e.g., using a least-squares procedure to match the nodal displacements calculated from (24) with those calculated directly from the solution of the global equations.

The above outlines the general formulation followed and is applicable to all the elements considered here. The specific details of the elements are now considered.

Figure 2 shows the element boundary approximations. The degrees of freedom at the four corners are the displacement and two rotations. These twelve degrees of freedom enable a unique linear variation of w, θ_x and θ_y on the boundary of the element to be achieved. To achieve quadratic and cubic variations on the boundary, extra degrees of freedom are introduced at the midside nodes. Shape functions associated with these degrees of freedom are conveniently taken as hierarchical [20] to enable the order of boundary approximations to be easily varied. However, traditional shape functions could also be used.

To ensure convergence to thin plate theory in the limit as the thickness approaches zero, the elements must be able to represent a quadratic variation in w and the associated linear variations in θ_x and θ_y. Thus, the lowest order element considered uses the twelve corner degrees of freedom plus four degrees of freedom associated with w at the midside nodes.

The elements are named according to the scheme *Qab-c* where a is the order of boundary approximation for w, b is the order of boundary approximation for θ_x and θ_y and c is the number of Trefftz solutions used. As the elements are hybrid-based, it is necessary (but not sufficient) for the resulting stiffness matrix to have full rank to use [12]

$$M \geq NDOF - 3 \tag{25}$$

where M is the number of Trefftz solutions used and $NDOF$ is the number of element degrees of freedom.

Table 1 summarizes the elements considered and their characteristics. As can be seen from the table, using the minimum number of Trefftz terms from (25) doesn't always guarantee an element with full rank. However, full rank can always be achieved by including more internal solutions as shown in the last column of the table. This does involve a computational penalty since the size of matrix $\boldsymbol{H}$ in (21), which must

be inverted numerically, increases.

The table also shows that not all the zero energy modes are commutable in a mesh. Moreover, the numerical tests detailed below show that, providing the structure is well supported, a global singularity doesn't occur. For this reason, the numerical results have concentrated on the use of the minimum number of Trefftz terms.

Element Q21-13, being the lowest order element, is of particular interest. This element may be stabilized by using 17 Trefftz terms. An alternative procedure is to use 15 Trefftz terms obtained by using the first 13 Trefftz terms from the generating sequence plus terms 16 and 17 from the sequence. This leads to an element with full rank which is denoted by Q21-15S. This procedure is slightly more efficient than using 17 Trefftz terms since matrix $\boldsymbol{H}$ is smaller. The numerical results given below show that there is little difference between elements Q21-13 and Q21-15S. Clearly, the same procedure could be used to develop stabilized versions of the other rank-deficient elements if desired.

5. NUMERICAL STUDIES

A detailed numerical evaluation of the proposed elements is given below. Unless noted otherwise, Poisson's ratio was taken as 0.3 and a shear correction factor of 5/6 was used.

Boundary conditions for thick plates are characterized as:

(1)	Clamped Support (C):	$w = \theta_t = \theta_n = 0$
(2)	Free Edge (F):	$M_n = M_{nt} = Q_n = 0$
(3)	Soft Simple Support (SS1):	$w = M_n = M_{nt} = 0$
(4)	Hard Simple Support (SS2):	$w = \theta_t = M_n = 0$

where the subscripts n and t refer to the normal and tangential directions at the plate boundary. In contrast to thin plate theory, where only the SS2 condition is permissible, thick plate theory allows two possible specifications of a simple support. The extra flexibility inherent in the SS1 condition proves beneficial where there is a danger of excessive constraint being induced by the SS2 condition. An example of this is the simply supported skew plate discussed below. Further discussion of this aspect is given in [3].

5.1 Patch Tests

Patch tests were performed on the elements using the mesh shown in Fig. 3. In all cases, the tests were performed by specifying values of the degrees of freedom on the exterior nodes consistent with the target stress state. The essembled patch equations were solved and internal displacements and stresses were compared with the exact values.

For a constant bending and twist state, a solution of the form

$$w = c_1 x^2 + c_2 xy + c_3 y^2 \tag{26.a}$$

$$\theta_x = 2c_1 x + c_2 y \tag{26.b}$$

$$\theta_y = c_2 x + 2c_3 y \tag{26.c}$$

is required to be represented for arbitrary constants c_1, c_2 and c_3. This solution is applicable for both thin and thick plates. All the elements passed this test exactly for all values of plate thickness, t.

The constant shear strain test is somewhat different. As noted in [9], this is a higher-order patch test for thin plate theory, i.e., it is not required to be satisfied for convergence. The difficulty is that a constant state of shear cannot exist without a corresponding linear variation in the moment field which is required from the equilibrium equations. Thus, this test is somewhat artificial.

To attempt to simulate a constant shear state, it is usual to impose a solution of the form

$$w = c_1 x + c_2 y \tag{27.a}$$

$$\theta_x = \theta_y = 0 \tag{27.b}$$

for arbitrary constants c_1 and c_2 on the patch. The exterior nodal variables are given values consistent with (27) and all θ_y and θ_y variables throughout the patch are set to zero.

Table 2 shows the results of such a test for varying values of t. It can be seen that the displacement at the typical point (4,7) in Fig. 3 approaches the value required by (27) as t increases. In addition, the internal shear stress approaches the correct constant value as t increases.

5.2 Simply Supported Plate

In this problem, a square simply supported (SS2) plate of size $a \times a$ and thickness t subjected to a uniform load p is considered. Taking symmetry into account, a quarter of the plate was analyzed using a uniform mesh of $N \times N$ elements. Results for the central displacement and bending moment for a thick plate ($a/t = 10$) and a thin plate ($a/t = 100$) are given in Tables 3-6.

It can be seen from the tables that all the elements yield converging results with increasing N. The lowest-order element, Q12-13, together with its stabilized version, Q21-15S, compare favourably with the higher-order elements. Element Q23-29, which uses a higher-order approximation for the rotations than for the displacements is perhaps the least convincing of the elements considered. It seems that the more natural approximation of using either equal approximations for the displacement and rotations or using an approximation one order higher for the displacement is preferable.

The tables, which concentrate on a single point in the mesh, don't give a true indication of the order of convergence of the elements. For this, it is preferable to study the strain energy variation with increasing N as given in Tables 7 and 8. Note that the tabulated values actually represent twice the strain energy as they were calculated using

$$U = \int_A pwdA \tag{28}$$

as was done in [10,21].

The energy error versus N is shown in Figures 4 and 5, enabling asymptotic energy convergence rates to be established. Also shown are the results for the DRM element [10]. It can be seen that while elements Q21-13, Q21-15S and DRM all have approximately the same convergence rate, elements Q21-13 and Q21-15S are more accurate. Increasing the boundary approximation, and correspondingly the order of internal approximations, results in better accuracy but not necessarily faster rates of convergence.

To demonstrate the lack of locking problems with the proposed elements, the plate was analyzed with a constant 8×8 mesh with increasing values of a/t. The results given in Table 9 show that none of the elements lock. Indeed, it is permissible to put

$t = 0$, while keeping D finite, without causing problems, as shown in the last line of the table. All elements rapidly converge to this limiting value as a/t is increased.

The sensitivity of the elements to mesh distortions is shown in Table 10. In this test a 2 × 2 mesh was used, with the central node being progressively moved from its original position at $(a/4, a/4)$ to a new position at $(a(1+\Delta)/4,\ a(1+\Delta)/4)$ for varying values of the distortion parameter, Δ. The results show that all the elements are relatively insensitive to mesh distortions. In particular, elements Q32-25 and Q33-33 are very insensitive to mesh distortions.

The prediction of shear stresses has been a continuing problem with thick plate elements, with some elements failing to give converging results [22,23]. It is typical to use some smoothing process to obtain satisfactory shear stresses, and a number of different schemes have been suggested [23–26].

For the present family, it was found that elements Q21-13, Q21-15S and Q32-21, i.e., those elements that use a higher-order approximation for w than for θ_x and θ_y, gave reliable values for shear stresses without any need for smoothing. The nodal values for the other elements became less reliable as the plate became thinner, although they gave satisfactory results for thick plates. In this regard, element Q23-29 performed worst whereas element Q33-33 gave reasonable results for an aspect ratio $a/t = 100$.

Several smoothing options were tried, namely:

(1) Calculating shears at the element centre only.

(2) Calculating shears at the 2 × 2 Gauss points and extrapolating using a bilinear equation.

(3) Smoothing the nodal bending moment field and calculating the shears from (3.a) assuming either a linear or quadratic variation of the moment field over the element.

(4) Taking the average shears over the element as being representative for the whole element [27].

Of the methods, method (3) was generally more accurate, although method (4) was also reliable. Tables 11 and 12 give results for the maximum shear force, Q_x, which occurs at point $(0, a/2)$. Where smoothing was used, the results quoted were obtained using method (3).

Finally, the plate was analyzed under a central point load, P. Mindlin's theory predicts an infinite deflection at the centre of the plate. Hence, results are only given for a thin plate using $a/t = 100$. The results given in Table 13 show that all the elements are converging to a value slightly higher than the thin plate value as expected.

5.3 Clamped Plate

A square clamped plate of size $a \times a$ and thickness t subjected to either a uniform load or a central point load was considered next. Again, using symmetry only a quarter of the plate was analyzed using a uniform mesh of $N \times N$ elements. Results are given in Tables 14–18 for both a thick and thin plate. All elements perform well.

5.4 Morley 30° Skew Plate

This problem [28] is a severe test case due to the singularity at the obtuse corners. Figure 6 shows the geometry of the problem together with a typical mesh ($N = 2$). To enable comparison with the results from [21], the shear correction factor was taken as one. The simple supports were treated using the SS1 condition.

Table 19 gives results for the central deflection, and includes the results for the DRM element for comparison. All elements appear to be converging to a higher value than the thin plate solution. As noted in [21], the thin plate model is in error by about 5% in terms of the average displacement with respect to a three-dimensional solution using the SS1 condition. Multiplying the thin plate value by 1.05 gives a value of 4.28 which is much closer to the results given in the table.

For this problem, the lower order elements perform better than the higher order elements. The smoother approximation used for the higher order elements is less able to cope with the singularity. However, better results could be achieved by

using a non-uniform mesh or by adding special singularity solutions to the internal approximations.

Table 20 gives the strain energy for the plate together with the three-dimensional value given in [21]. Again, it can be seen that the lower order elements are performing better. However, in view of the difficulty of the problem, the results are quite good.

5.5 Circular Plate with Central Hole

As a final example, a circular plate with a central hole, clamped on the outer boundary and subjected to a uniform load is considered. Using symmetry, a quarter of the plate was analyzed. Figure 7 shows the region considered together with a typical mesh ($N = 2$).

Tables 21 and 22 give results for the maximum displacement and moment. In this problem, the geometric error is significant as shown in the results. The higher order elements overconstrain the problem on the interpolated clamped boundary more than the lower order elements. This problem can be alleviated by using curved elements or the procedure suggested in [29].

6. CONCLUSIONS

The Hybrid-Trefftz method has been extended to enable the analysis of thick plates to be performed. Exact solutions of Mindlin's equations have been derived which are used as the internal element approximations. Using varying orders of boundary approximations enables a family of quadrilateral elements to be derived. The formulation results in a standard stiffness formulation making the elements easily integrated into a displacement-based finite element program. The numerical results presented demonstrated the good accuracy achieved by the elements.

Extensions of the present work are possible. In particular, the procedure can be used to develop triangular elements and elements with curved sides. The inclusion of special functions to model singularity problems also seems desirable. These aspects will be considered further.

ACKNOWLEDGEMENT

This work was carried out while visiting the Texas Institute for Computational Mechanics. The author wishes to thank Professor J. T. Oden for making the visit possible, and for the use of the Institute's facilities.

REFERENCES

[1] R. D. Mindlin, Influence of rotatory inertia and shear on flexural motion of isotropic plates, J. Appl. Mech. 18 (1951) 31-38.

[2] O. C. Zienkiewicz, *The Finite Element Method*, 3rd Edition, Mc-Graw Hill, London, 1977.

[3] T. J. R. Hughes, *The Finite Element Method: Linear, Static and Dynamic Finite Element Analysis*, Prentice Hall, Englewood Cliffs, N.J., 1987.

[4] T. J. R. Hughes, and E. Hinton, *Finite Element Methods for Plate and Shell Structures, Volume 1: Element Technology*, Pineridge Press, Swansea, 1986.

[5] M. A. Crisfield, *Finite Elements and Solution Procedures for Structural Analysis, Volume 1: Linear Analysis*, Pineridge Press, Swansea, 1986.

[6] R. D. Cook, D. S. Malkus, and M. E. Plesha, *Concepts and Applications of Finite Element Analysis*, 3rd Edition, Wiley, N.Y., 1989.

[7] K. J. Bathe and E. N. Dvorkin, A four node plate bending element based on Mindlin/Reissner plate theory and mixed interpolation, Int. J. Numer. Meths. Engrg. 21(2) (1985) 367-383.

[8] H. C. Huang and E. Hinton, A nine node Lagrangian Mindlin element with enhanced shear interpolation, Engrg. Comp. 1(4) (1984) 77-88.

[9] J. L. Batoz and P. Lardeur, A discrete shear triangular nine D.O.F. element for the analysis of thick to very thin plates, Int. J. Numer. Meths. Engrg. 28(3) (1989) 533-560.

[10] O. C. Zienkiewicz, R. L. Taylor, P. Padadopoulos and E. Oñate, Plate bending elements with discrete constraints: new triangular elements, Comp. Struct. (to appear).

[11] J. Jirousek and N. Leon, A powerful finite element for plate bending, Comp. Meth. Appl. Mech. Engrg. 12(1) (1977) 77-96.

[12] T. H. H. Pian, and P. Tong, Basis of finite element methods for solid continua, Int. J. Numer. Meths. Engrg. 1(1) (1969) 3-28.

[13] J. Jirousek and P. Teodorescu, Large finite elements for the solution of problems in the theory of elasticity, Comp. Struct. 15(5) (1982) 575-587.

[14] J. Jirousek and L. Guex, The Hybrid-Trefftz finite element model and its application to plate bending, Int. J. Numer. Meths. Engrg. 23(4) (1986) 651-693.

[15] J. Jirousek, Hybrid-Trefftz plate bending elements with p-method capabilities, Int. J. Numer. Meths. Engrg. 24(7) (1987) 1367-1393.

[16] J. Petrolito, A modified ACM element for thick plate analysis, Comp. Struct. (to appear).

[17] H. Reismann, *Elastic Plates: Theory and Application*, Wiley, N.Y., 1988.

[18] R. Szilard, *Theory and Analysis of Plates*, Prentice Hall, Englewood Cliffs, N.J., 1974.

[19] J. Petrolito and B. W. Golley, Plate bending analysis using macro elements, Comp. Struct. 28(3) (1988) 407-419.

[20] O. C. Zienkiewicz and R. L. Taylor, *The Finite Element Method, Volume 1: Basic Formulation and Linear Problems*, 4th Edition, Mc-Graw Hill, London, 1989.

[21] I. Babuška and T. Scapolla, Benchmark computation and performance evaluation for a rhombic plate bending problem, Int. J. Numer. Meths. Engrg. 28(1) (1989) 155-179.

[22] K. J. Bathe and F. Brezzi, On the convergence of a four-node plate bending element based on Mindlin/Reissner plate theory and a mixed interpolation, in *Mathematics of Finite Elements and Applications*, (J. R. Whiteman, editor), Academic Press, London (1985) 491-503.

[23] T. J. R. Hughes and L. P. Franca, Convergence of transverse shear stresses in the finite element analysis of plates, Com. Appl. Numer. Meths. 4(2) (1988) 185-187.

[24] M. Mukhopadhay, Analysis of plates using isoparametric quadratic element–shear, reaction, patch loading and some convergence studies, Comp. Struct. 17(4) (1983) 587-597.

[25] J. Jirousek and A. Bouberguig, A contribution to evaluation of shear forces and reactions of Mindlin plates using isoparametric elements, Comp. Struct. 19(5/6) (1984) 793-800.

[26] J. Jirousek, Comment on evaluation of shear forces and reactions from transverse shear deformations by using isoparametric quadratic Mindlin plate elements, Comp. Struct. 19(5/6) (1984) 899-903.

[27] G. F. Carey, Private communication, 1989.

[28] L. S. D. Morley, *Skew Plates and Structures*, Pergamon Press, London, 1963.

[29] H. Stolarski, N. Carpenter and T. Belytschko, A Kirchhoff-mode method for C^0 bilinear and serendipity plate elements, Comp. Meth. Appl. Mech. Engrg., 50(2) (1985) 121-145.

TABLE 1
Summary of elements

Element	No. of zero energy modes	Type of zero energy mode[a]	Minimum no. of Trefftz terms for full rank
Q21-13	2	1N+1C	17
Q21-15S	0	-	15
Q22-21	0	-	21
Q32-25	3	3N[b]	33
Q23-29	0	-	29
Q33-33	1	N	35

[a] N = non-commutable with a mesh of two or more elements;
C = commutable.

[b] With a minimum 2 × 2 mesh; a 2 × 1 mesh has 1 zero energy mode.

TABLE 2
Displacement at point (4,7) in Fig. 3 for shear patch test ($c_1 = 1$, $c_2 = 0$, exact value = 4.000)

t	Q21-13	Q21-15S	Q22-21	Q32-25	Q23-29	Q33-33
0.1	2.975	4.510	4.364	4.434	4.351	4.358
1	3.155	4.277	4.147	4.188	4.140	4.167
10	3.968	3.998	3.993	3.995	3.993	3.997
100	4.000	4.000	4.000	4.000	4.000	4.000

TABLE 3
Central displacement for simply supported (SS2) plate subjected to uniform load ($a/t = 10$, exact value = 4.2728, multiplier = $10^{-3}pa^4/D$)

N	Q21-13	Q21-15S	Q22-21	Q32-25	Q23-29	Q33-33
1	4.3855	4.1774	4.2914	4.2678	4.2696	4.2634
2	4.3268	4.2685	4.2719	4.2727	4.2713	4.2725
4	4.2873	4.2734	4.2727	4.2728	4.2727	4.2728
8	4.2765	4.2731	4.2728	4.2728	4.2728	4.2728
16	4.2738	4.2729	4.2728	4.2728	4.2728	4.2728

TABLE 4
Central moment for simply supported (SS2) plate subjected to uniform load ($a/t = 10$, exact value = 4.7886, multiplier = $10^{-2}pa^2$)

N	Q21-13	Q21-15S	Q22-21	Q32-25	Q23-29	Q33-33
1	4.7086	5.0900	5.3185	4.7608	5.6328	4.6202
2	4.7856	4.8597	4.8547	4.7885	4.8666	4.7821
4	4.7884	4.7939	4.7934	4.7887	4.7940	4.7883
8	4.7886	4.7890	4.7889	4.7886	4.7890	4.7886
16	4.7886	4.7887	4.7887	4.7886	4.7887	4.7886

TABLE 5
Central displacement for simply supported (SS2) plate subjected to uniform load ($a/t = 100$, exact value = 4.0645, multiplier = $10^{-3}pa^4/D$)

N	Q21-13	Q21-15S	Q22-21	Q32-25	Q23-29	Q33-33
1	4.1545	3.8994	3.9995	4.0594	3.9742	4.0675
2	4.1157	4.0245	4.0404	4.0643	4.0400	4.0648
4	4.0787	4.0554	4.0586	4.0645	4.0583	4.0645
8	4.0681	4.0629	4.0634	4.0645	4.0633	4.0645
16	4.0654	4.0643	4.0643	4.0645	4.0643	4.0645

TABLE 6
Central moment for simply supported (SS2) plate subjected to uniform load ($a/t = 100$, exact value = 4.7886, multiplier = $10^{-2}pa^2$)

N	Q21-13	Q21-15S	Q22-21	Q32-25	Q23-29	Q33-33
1	4.7201	5.3799	6.1246	4.7010	6.5882	4.2588
2	4.7873	5.1106	5.0749	4.7881	5.0698	4.7137
4	4.7886	4.8581	4.8522	4.7886	4.8540	4.7781
8	4.7887	4.8011	4.8003	4.7886	4.8013	4.7873
16	4.7886	4.7902	4.7901	4.7886	4.7902	4.7885

TABLE 7
Strain energy per quarter plate for simply supported (SS2) plate subjected to uniform load
($a/t = 10$, exact value = 4.507307, multiplier = $10^{-4}pa^6/D$)

N	Q21-13	Q21-15S	Q22-21	Q32-25	Q23-29	Q33-33
1	4.687513	4.335979	4.464171	4.466164	4.466348	4.498563
2	4.566597	4.490108	4.498522	4.503105	4.499811	4.506793
4	4.522423	4.505524	4.506469	4.507011	4.506607	4.507280
8	4.511071	4.507061	4.507247	4.507288	4.507258	4.507305
16	4.508246	4.507259	4.507303	4.507306	4.507304	4.507307

TABLE 8
Strain energy per quarter plate for simply supported (SS2) plate subjected to uniform load
($a/t = 100$, exact value = 4.258787, multiplier = $10^{-4}pa^6/D$)

N	Q21-13	Q21-15S	Q22-21	Q32-25	Q23-29	Q33-33
1	4.372908	4.086967	4.204351	4.222795	4.185119	4.242103
2	4.310642	4.213955	4.228028	4.254861	4.223954	4.257252
4	4.273256	4.247063	4.249651	4.258481	4.248921	4.258690
8	4.262492	4.256472	4.256977	4.258766	4.256884	4.258782
16	4.259718	4.258478	4.258562	4.258785	4.258554	4.258786

TABLE 9
Effect of varying a/t values on central displacement of simply supported (SS2) plate subjected to uniform load
($N = 8$, thin plate value = 4.0624, multiplier = $10^{-3}pa^4/D$)

a/t	Q21-13	Q21-15S	Q22-21	Q32-25	Q23-29	Q33-33
10	4.3855	4.1774	4.2914	4.2678	4.2696	4.2634
10^2	4.1545	3.8994	3.9995	4.0594	3.9742	4.0675
10^3	4.0660	4.0598	4.0607	4.0624	4.0606	4.0624
10^4	4.0660	4.0597	4.0607	4.0624	4.0605	4.0624
∞	4.0660	4.0597	4.0607	4.0624	4.0605	4.0624

TABLE 10

Percentage change in central displacement of simply supported (SS2) plate subjected to uniform load for distorted mesh relative to value for undistorted mesh ($N = 2$, $a/t = 10$)

Δ	Q21-13	Q21-15S	Q22-21	Q32-25	Q23-29	Q33-33
0.1	0.19	0.06	0.03	0.00[a]	0.04	0.00
0.2	0.44	0.33	0.11	0.01	0.14	0.00
0.3	0.81	0.83	0.25	0.01	0.31	0.00
0.4	1.36	1.61	0.46	0.02	0.57	0.01
0.5	2.19	2.72	0.77	0.03	0.94	0.01

[a] "Zero" = less than 5×10^{-3}

TABLE 11

Shear force Q_x at point $(0, a/2)$ for simply supported (SS2) plate subjected to uniform load ($a/t = 10$, exact value = 3.3765, multiplier = $10^{-1}pa$)

N	Q21-13[a]	Q21-15S[a]	Q22-21[a]	Q22-21[b]	Q32-25[a]	Q23-29[a]	Q23-29[b]	Q33-33[a]	Q33-33[b]
1	2.9483	1.8965	4.1625	2.5550	3.0914	5.1261	2.8402	4.0386	3.0950
2	3.3799	3.2240	4.3716	2.9843	3.3486	4.6245	3.2607	3.5537	3.2514
4	3.3717	3.3492	3.8346	3.1994	3.3707	3.8760	3.3653	3.4078	3.3429
8	3.3757	3.3724	3.5235	3.2909	3.3755	3.5293	3.3777	3.3811	3.3681
16	3.3764	3.3759	3.4175	3.3334	3.3764	3.4183	3.3775	3.3772	3.3744

[a] Nodal value
[b] Smoothed value - quadratic

TABLE 12

Shear force Q_x at point $(0, a/2)$ for simply supported (SS2) plate subjected to uniform load ($a/t = 100$, exact value = 3.3765, multiplier = $10^{-1}pa$)

N	Q21-13[a]	Q21-15S[a]	Q22-21[b]	Q22-21[c]	Q32-25[a]	Q23-29[b]	Q23-29[c]	Q33-33[b]	Q33-33[c]
1	2.7819	1.0077	1.8177	1.9803	2.7602	2.0505	2.4850	1.5856	3.0457
2	3.4051	2.9453	2.6891	2.9343	3.7543	2.6076	2.9545	2.3544	3.1710
4	3.3610	3.1642	3.0625	3.2364	3.6076	3.0169	3.2633	2.8072	3.3084
8	3.3719	3.2637	3.2182	3.3941	3.4354	3.2387	3.5514	3.0771	3.3593
16	3.3757	3.3451	3.2765	3.4111	3.3807	3.3071	3.5487	3.2236	3.3729

[a] Nodal value
[b] Smoothed value - linear
[c] Smoothed value - quadratic

TABLE 13
Central displacement for simply supported (SS2) plate subjected to point load ($a/t = 100$, thin plate value = 1.1160, multiplier = Pa^2/D)

N	Q21-13	Q21-15S	Q22-21	Q32-25	Q23-29	Q33-33
1	1.2782	1.1762	1.1917	1.1892	1.1631	1.1796
2	1.2135	1.1562	1.1564	1.1691	1.1498	1.1668
4	1.1806	1.1591	1.1592	1.1643	1.1577	1.1639
8	1.1692	1.1616	1.1622	1.1619	1.1619	1.1633
16	1.1660	1.1627	1.1631	1.1630	1.1631	1.1633

TABLE 14
Central displacement for clamped plate subjected to uniform load ($a/t = 10$, multiplier = $10^{-3}pa^4/D$)

N	Q21-13	Q21-15S	Q22-21	Q32-25	Q23-29	Q33-33
1	1.4507	1.3899	1.5110	1.4984	1.4552	1.4892
2	1.5150	1.4740	1.4985	1.5079	1.4973	1.5076
4	1.5103	1.4987	1.5057	1.5067	1.5058	1.5069
8	1.5062	1.5032	1.5055	1.5056	1.5055	1.5056
16	1.5050	1.5043	1.5049	1.5049	1.5049	1.5050

TABLE 15
Central moment for clamped plate subjected to uniform load ($a/t = 10$, multiplier = $10^{-2}pa^2$)

N	Q21-13	Q21-15S	Q22-21	Q32-25	Q23-29	Q33-33
1	2.2358	2.4073	3.3266	2.2968	3.8653	2.0055
2	2.3295	2.4005	2.4331	2.3229	2.4526	2.3122
4	2.3251	2.3301	2.3294	2.3220	2.3307	2.3216
8	2.3214	2.3216	2.3214	2.3209	2.3215	2.3209
16	2.3203	2.3203	2.3203	2.3203	2.3203	2.3203

TABLE 16
Central displacement for clamped plate subjected to uniform load ($a/t = 100$, thin plate value = 1.26, multiplier = $10^{-3}pa^4/D$)

N	Q21-13	Q21-15S	Q22-21	Q32-25	Q23-29	Q33-33
1	1.2098	1.1413	1.0598	1.2544	0.9604	1.2609
2	1.2524	1.1915	1.1822	1.2657	1.1782	1.2674
4	1.2638	1.2456	1.2456	1.2677	1.2443	1.2678
8	1.2674	1.2632	1.2637	1.2679	1.2635	1.2679
16	1.2679	1.2670	1.2674	1.2679	1.2673	1.2679

TABLE 17
Central moment for clamped plate subjected to uniform load ($a/t = 100$, thin plate value = 2.31, multiplier = $10^{-2}pa^2$)

N	Q21-13	Q21-15S	Q22-21	Q32-25	Q23-29	Q33-33
1	2.1793	2.4759	4.7655	2.1885	5.6018	1.1730
2	2.2775	2.5753	2.7197	2.2905	2.6978	2.1574
4	2.2856	2.3537	2.3826	2.2907	2.3852	2.2735
8	2.2901	2.3020	2.3077	2.2909	2.3092	2.2889
16	2.2909	2.2923	2.2930	2.2910	2.2932	2.2908

TABLE 18
Central displacement for clamped plate subjected to point load ($a/t = 100$, thin plate value = 5.60, multiplier = $10^{-3}Pa^2/D$)

N	Q21-13	Q21-15S	Q22-21	Q32-25	Q23-29	Q33-33
1	6.2305	5.7729	5.6264	5.8879	5.0978	5.8072
2	5.9717	5.4982	5.4713	5.6994	5.4027	5.6801
4	5.7757	5.5759	5.5754	5.6549	5.5587	5.6509
8	5.6954	5.6225	5.6288	5.6456	5.6259	5.6452
16	5.6701	5.6381	5.6424	5.6456	5.6422	5.6456

TABLE 19
Central displacement for Morley skew plate
($a/t = 100$, thin plate value = 4.08, multiplier = $10^{-4}pa^4/D$)

N	Q21-13	Q21-15S	Q22-21	Q32-25	Q23-29	Q33-33	DRM
2	4.5206	4.1380	5.3930	4.8548	4.9782	5.0863	6.2674
4	4.4816	4.2381	4.5540	4.5964	4.5770	4.7561	4.5375
8	4.3913	4.2973	4.4832	4.5055	4.5240	4.5700	4.2546
16	4.2958	4.2582	4.4177	4.3868	4.3890	4.4180	4.2134

TABLE 20
Strain energy for Morley skew plate ($a/t = 100$, 3-D value [21] = 7.304074, multiplier = $10^{-5}pa^6/D$)

N	Q21-13	Q21-15S	Q22-21	Q32-25	Q23-29	Q33-33	DRM
2	8.501009	7.266239	13.634564	12.292063	13.334414	14.057814	7.832500
4	7.792962	7.376286	8.200199	8.241384	8.324208	8.537150	7.058874
8	7.520923	7.380548	7.687949	7.723813	7.748876	7.825085	7.178269
16	7.363927	7.309361	7.486250	7.505414	7.488175	7.552492	7.210302

TABLE 21
Maximum displacement for circular plate
($a/t = 100$, thin plate value = 5.27, multiplier = $10^{-3}pa^4/D$)

N	Q21-13	Q21-15S	Q22-21	Q32-25	Q23-29	Q33-33
2	5.4719	3.7191	3.7499	3.7197	3.7740	3.7706
4	5.1953	4.8366	4.8779	4.9606	4.8777	4.8805
8	5.2448	5.1606	5.1755	5.1758	5.1751	5.1757
16	5.2645	5.2447	5.2483	5.2483	5.2482	5.2482
24	5.2685	5.2601	5.2614	5.2614	5.2614	5.2614

TABLE 22

Maximum moment for circular plate

($a/t = 100$, thin plate value = 8.00, multiplier = $10^{-2}pa^2$)

N	Q21-13	Q21-15S	Q22-21	Q32-25	Q23-29	Q33-33
2	8.3695	3.7331	1.9765	2.0237	1.2343	1.2739
4	8.0840	6.4614	4.9461	4.8779	4.2618	4.1726
8	8.0446	7.4315	6.5660	6.5980	6.2341	6.2012
16	8.0236	7.8033	7.3976	7.4184	7.3060	7.2948
24	8.0159	7.9085	7.6725	7.6840	7.6359	7.6295

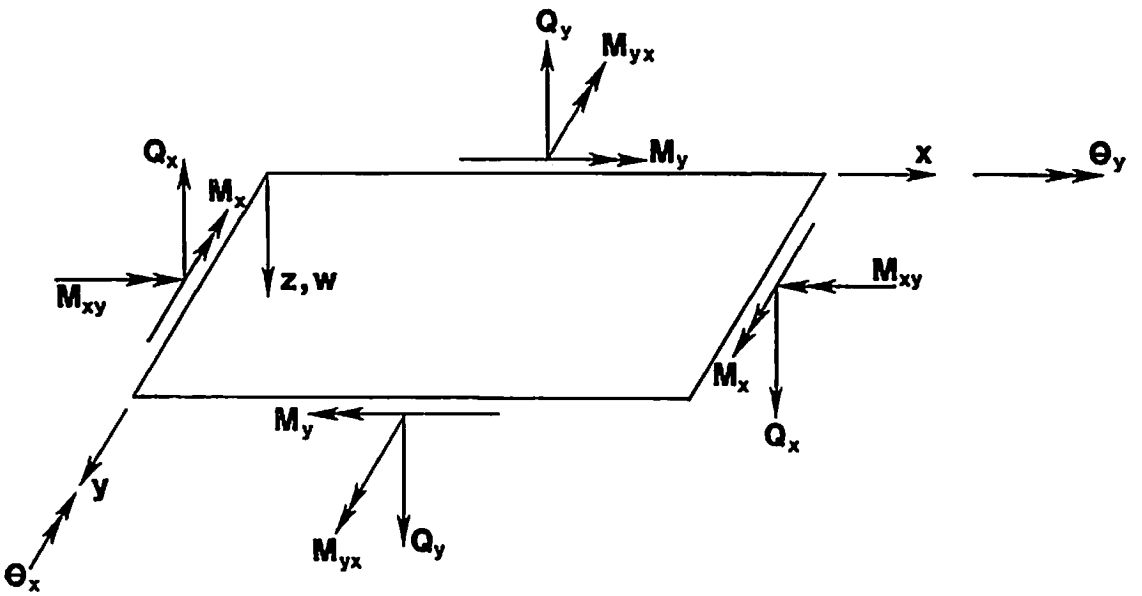

Fig. 1 Sign convention

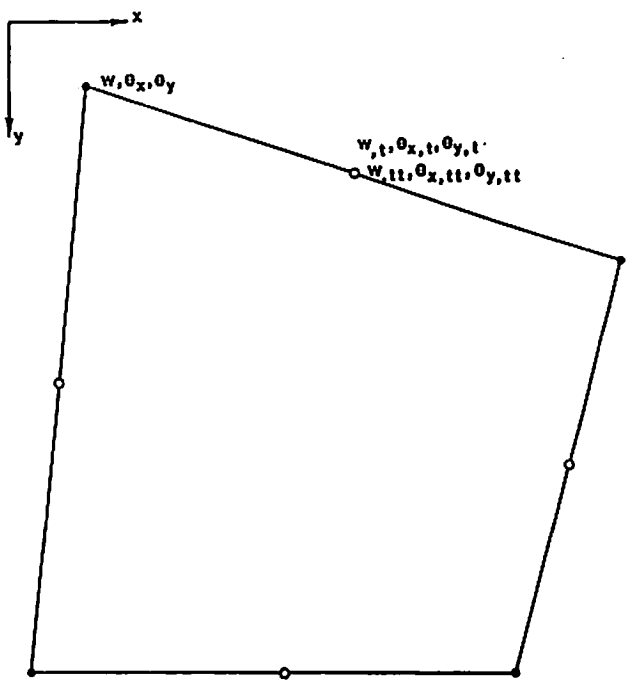

Fig. 2 Geometry and degrees of freedom for elements

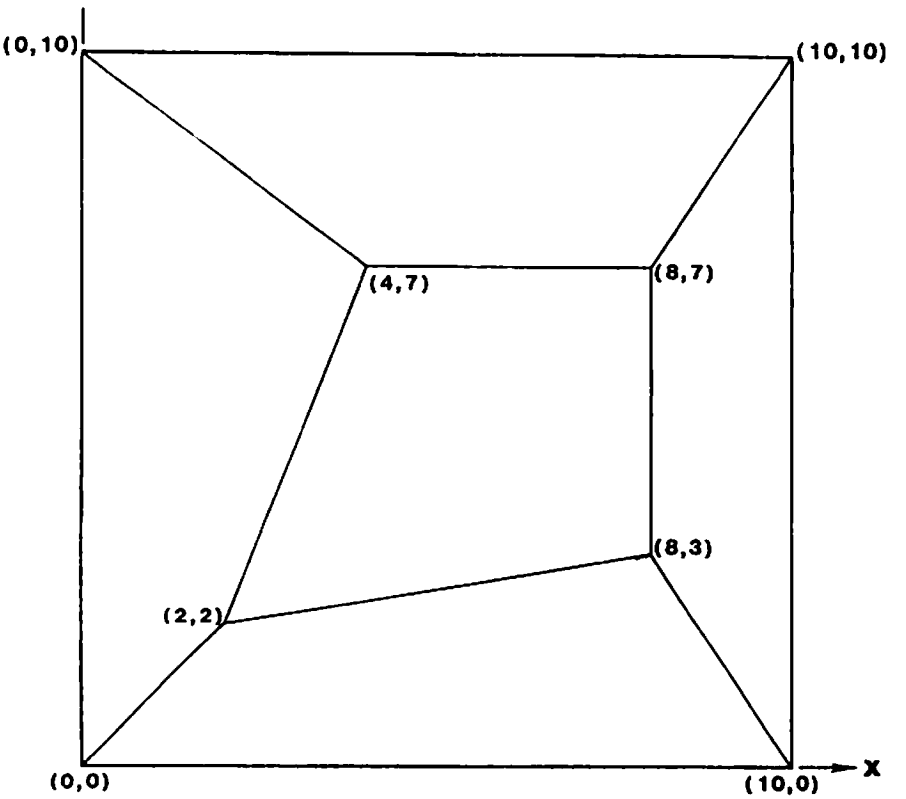

Fig. 3 Patch test geometry

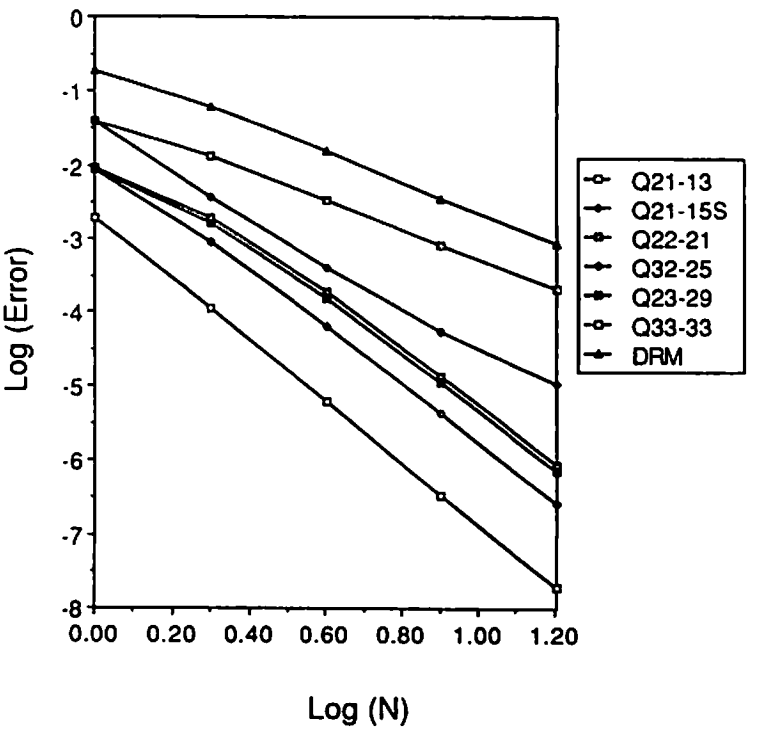

Fig. 4 Energy errors for simply supported plate subjected to uniform load ($a/t = 10$)

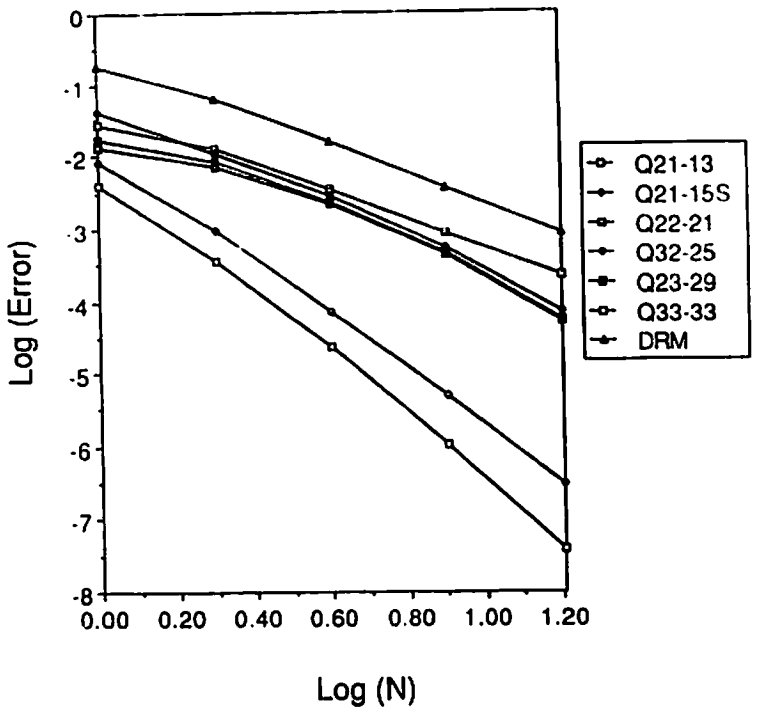

Fig. 5 Energy errors for simply supported plate subjected to uniform load ($a/t = 100$)

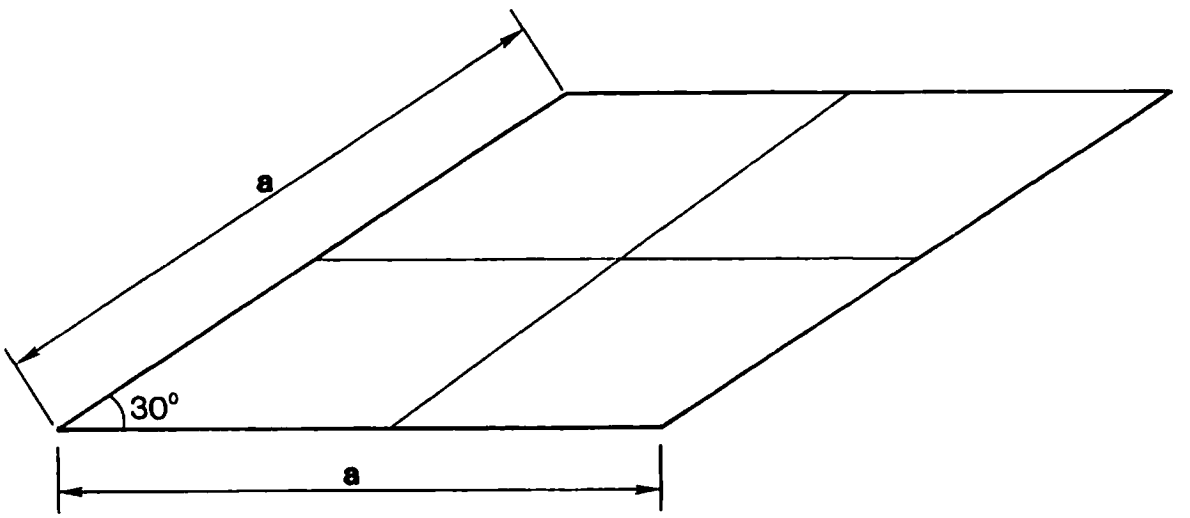

Fig. 6 Morley's skew plate problem and typical mesh ($N = 2$)

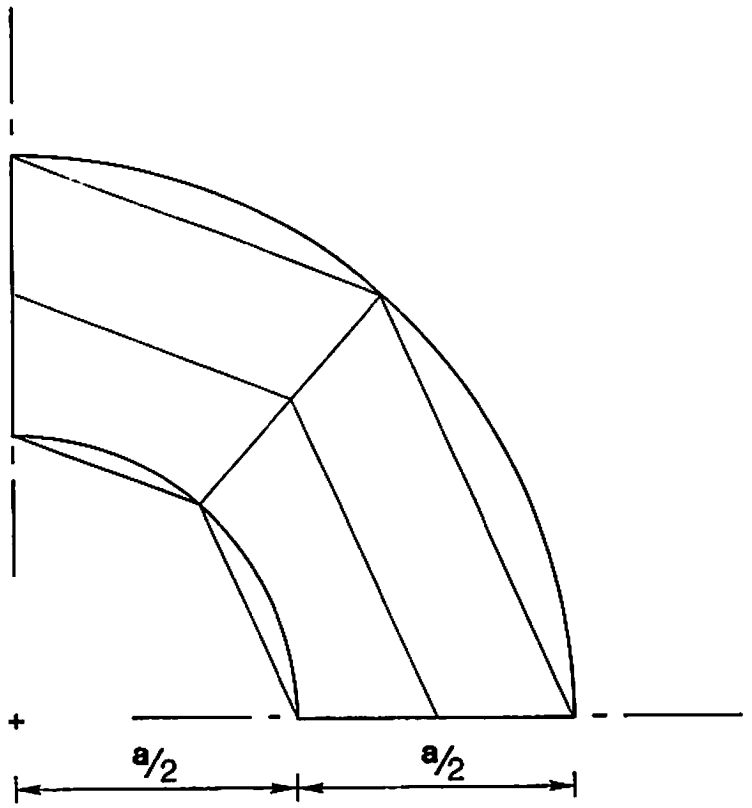

Fig. 7 Circular plate with hole problem and typical mesh ($N = 2$)